Eur. Phys. J. Appl. Phys. **92**, 31101 (2020)

https://doi.org/10.1051/epjap/2020200286

THE EUROPEAN PHYSICAL JOURNAL APPLIED PHYSICS

Regular Article

Burgers fluid flow in perspective of Buongiorno's model with improved heat and mass flux theory for stretching cylinder★

Zahoor Iqbal*, Masood Khan, and Awais Ahmed

Department of Mathematics, Quaid-i-Azam University, Islamabad 44000, Pakistan

Received: 10 September 2020 / Received in final form: 17 October 2020 / Accepted: 19 October 2020

Abstract. In this study, an effort is made to model the thermal conduction and mass diffusion phenomena in perspective of Buongiorno's model and Cattaneo-Christov theory for 2D flow of magnetized Burgers nanofluid due to stretching cylinder. Moreover, the impacts of Joule heating and heat source are also included to investigate the heat flow mechanism. Additionally, mass diffusion process in flow of nanofluid is examined by employing the influence of chemical reaction. Mathematical modelling of momentum, heat and mass diffusion equations is carried out in mathematical formulation section of the manuscript. Homotopy analysis method (HAM) in Wolfram Mathematica is utilized to analyze the effects of physical dimensionless constants on flow, temperature and solutal distributions of Burgers nanofluid. Graphical results are depicted and physically justified in results and discussion section. At the end of the manuscript the section of closing remarks is also included to highlight the main findings of this study. It is revealed that an escalation in thermal relaxation time constant leads to ascend the temperature curves of nanofluid. Additionally, depreciation is assessed in mass diffusion process due to escalating amount of thermophoretic force constant.

1 Introduction

Non-Newtonian fluids are of great importance due to their wonderful heat transform features and applications in engineering systems like, heat exchangers, solution suspensions, food processing systems, biochemical progressing and geophysical developments. There are different non-Newtonian fluid models which exhibit the behavior of non-Newtonian fluids. These models comprise differential, integral and rate type fluid models. Rate type models are further subcategorized as Maxwell, Oldroyd-B and Burgers fluid models. Burgers model is considered as the comprehensive viscoelastic rate type fluid model which delineates the complete features of non-Newtonian fluids. Burgers fluid model explains the relaxation and retardation time properties of fluid and this model also elucidates the movement of earth's mantle. Regardless of its countless applications, Burgers fluid model has not gained considerable consideration in the past. But, some work on Burgers fluid model has done in past which we mention here like, Ravindran et al. [1] investigated the flow of Burgers fluid between two parallel surfaces which are rotating along non-coincident axes. Hayat et al. [2] examined the simple flow of a Burgers fluid. Additionally, Hayat [3] inspected the rotational Burgers fluid flow due to a flat surface. He found that the velocity of fluid initially grows up and then depreciates afterwards. Khan et al. [4] examined the flow of Burgers fluid in a pipe by considering the effects of Hall current. They disclosed that the flow curves of Burgers magnetic fluid build up for higher scales of Hall parameter. Moreover, Hayat et al. [5] presented a mathematical model to study the flow of Burgers fluid due to a stretching sheet. Hayat et al. [6] explored the flow of magneto Burgers fluid in view of heat source. They observed that the flow distribution of nanofluid escalates due to growing magnitude of retardation time parameter. Khan et al. [7] analyzed the boundary layer flow of Burgers nanofluid with the effects of nonlinear radiation. They reported that the thermal distribution of nanofluid rises for improving scales of radiation constant. Recently, Waqas et al. [8] employed the non-Fourier's and Fick's laws to study the heat transform features in flow of Burgers fluid due to stretching surface. Khan et al. [9] examined the flow of Burgers fluid near a stagnation point by incorporating the effects of thermal radiation. They exposed that the fluid velocity builds up by intensifying the scales of velocity ratio parameter. Iqbal et al. [10] investigated the magneto Burgers nanofluid by employing modified heat and mass fluxes over a stretchable sheet. They noted that the thermal energy flow deteriorates for higher scales of thermal relaxation parameter.

Nanofluids gained so much importance during past two decades due to their astounding performance in thermal conduction and a variety of applications in industries and advancement of electronic devices. Nanofluids structure comprises very micro size particles in the base fluid. Commonly used particles are in the base fluid are carbides, oxides, metals and carbon nanotubes etc.

★Contribution to the Topical Issue "Advanced Materials for Energy Harvesting, Storage, Sensing and Environmental Engineering (ICOME 2019)", edited by Mohammed El Ganaoui, Mohamed El Jouad, Rachid Bennacer, Jean-Michel Nunzi.

* e-mail: izahoor@math.qau.edu.pk

Nanofluids are extensively used in cooling process of refrigerators, engines, air conditioners, transformers and other electronic devices. Due to such diverse practical implementations, researchers contributed a lot by doing theoretical analysis on different types of nanofluids with different thermophysical features. Earlier, Masuda et al. [11] examined the thermal conductivity of nanofluids and they reported that nanofluid contains the higher thermal conductivity as compared to their respective base fluid. The thermal properties of copper based nanofluids were then examined by Choi [12] and Choi et al. [13]. They informed that the nanofluids possess very high thermal conductivity as compared to conventional fluids. The fact is that nanofluids contains metal particles and we know that the thermal conductivity of metals is much higher than usual fluids. So that they incorporated the tiny particles of copper into usual fluids and formed nanofluids and examined experimentally in lab and they came to know the interesting results that nanofluids are much better than base fluids due to higher thermal conduction features. Moreover, Yoo et al. [14] also experimentally examined the thermophysical features of nanofluid based on Iron (Fe), Aluminum oxide (Al_2O_3), Titanium dioxide (TiO_2) and tungsten trioxide (WO_3) nanomaterials. They also expressed that the nanofluid with such particles also exhibit very higher thermal conductivity as compared to base fluid. Later on, Buongiorno [15] presented a model consists of the process of thermophoresis and Brownian diffusion to examine the thermal conduction features of nanofluids. In his experiment, he observed that only Brownian motion and thermophoresis are significant slip mechanisms for nanofluids out of seven slip mechanisms. Philip et al. [16] studied thermal features of nanofluid. Khan and Pop [17] inspected the nanofluid flow due to stretching material. Turkyilmazoglu [18–20] examined the heat transfer mechanism in flow of nanofluid for vertical and rotating geometries. Hsiao [21] explored the multimedia features of nanofluid flow with radiation effects. Sheikholeslami et al. [22,23] discussed the thermal features in convective flows of nanofluid by considering the effects of magnetic field. Hsiao [24,25] scrutinized the flows of nanofluids by incorporating the influences of activation energy and viscous dissipation. Sheikholeslami et al. [26–28] explored the different types of nanofluids with different base fluids with considering other physical effects on different geometries. Some other investigation on nanofluids are mentioned in references [29–32].

From the above mentioned studies we inspected that the flow of Burgers fluid is still not investigated by employing Cattaneo-Christov heat and mass diffusion theory in combination with Buongiorno's model for stretching cylinder case. Therefore, this article is designed to study the heat transport and mass diffusion process in flow of Burgers nanofluid caused by stretching cylinder and by utilizing Cattaneo-Christov theory and Buongiorno's model. The effects of Lorentz force in the flow and the effect of Joule heating in the heat equation are also considered. The effects of productive and destructive chemical reactions are also incorporated to investigate the mass diffusion process. Homotopic approach is being utilized to check the behavior of physical constraints. The impact of different physical parameters is depicted through graphs.

2 Mathematical formulation

We are considering 2D axisymmetric flow of Burgers nanofluid with the effect of uniform magnetic field which is applied in the direction normal to the flow. The flow under discussion is further considered as steady and incompressible. Moreover, it is assumed that the flow is conducted by stretching the boundary of the cylinder along $z-axis$ with stretching velocity $w = \frac{U_0 z}{l}$. Here U_0 represents the reference velocity and l denotes the specific length. We are considering cylindrical polar coordinates (r, θ, z) to model the flow, temperature and concentration equations. Here, $z-axis$ is taken along the axis of the cylinder while $r-axis$ is considered along the normal to the flow direction, i.e, radial direction as depicted in Figure 1. Here, $\mathbf{V} = [u, 0, w]$ is taken as the velocity field for the flow where, the velocities along r and z directions are represented by u and w, respectively. Furthermore, the flow of Burgers nanofluid is modelled in terms of uniform magnetic field of strength $\mathbf{B} = [B_0, 0, 0,]$. Additionally, the equation representing the heat transport in the flow of nanofluid is modelled by employing the Cattaneo-Christov heat flux in addition with the effects of Joule heating and heat source/sink. The concentration of nanoparticles is modelled by utilizing modified mass flux and the effect of chemical reaction. Furthermore, (T_w, C_w) are considered as the temperature and concentration at the wall of the cylinder respectively.

The equations of continuity, flow, temperature and concentration for the present problem are given below

$$\frac{\partial u}{\partial r} + \frac{u}{r} + \frac{\partial w}{\partial z} = 0, \tag{1}$$

See equation (2) next page.

See equation (3) next page.

$$\begin{aligned} & u\frac{\partial C}{\partial r} + w\frac{\partial C}{\partial z} - \frac{D_t}{T_\infty}\left(\frac{\partial^2 T}{\partial r^2} + \frac{1}{r}\frac{\partial T}{\partial r}\right) \\ & +\lambda_c\left[\begin{array}{c} u^2\frac{\partial^2 C}{\partial r^2} + w^2\frac{\partial^2 C}{\partial z^2} + 2uw\frac{\partial^2 C}{\partial r \partial z} + u\frac{\partial u}{\partial r}\frac{\partial C}{\partial r} \\ +u\frac{\partial w}{\partial r}\frac{\partial C}{\partial z} + w\frac{\partial u}{\partial z}\frac{\partial C}{\partial r} + w\frac{\partial w}{\partial z}\frac{\partial C}{\partial z} \end{array}\right] \\ & = D_b\left[\frac{\partial^2 C}{\partial r^2} + \frac{1}{r}\frac{\partial C}{\partial r}\right] + \lambda_c\frac{D_t}{T_\infty}\left(u\frac{\partial^3 T}{\partial r^3} + \frac{u}{r^2}\frac{\partial T}{\partial r}\right. \\ & \left. +\frac{u}{r}\frac{\partial^2 T}{\partial r^2} + w\frac{\partial^3 T}{\partial r^2 \partial z} + \frac{w}{r^2}\frac{\partial^2 T}{\partial r \partial z}\right) \\ & -K_c\left[(C - C_\infty) + \lambda_c\left(u\frac{\partial C}{\partial r} + w\frac{\partial C}{\partial z}\right)\right], \end{aligned} \tag{4}$$

$$
\begin{aligned}
&u\frac{\partial w}{\partial r}+w\frac{\partial w}{\partial z}+\lambda_1\left[u^2\frac{\partial^2 w}{\partial r^2}+w^2\frac{\partial^2 w}{\partial z^2}+2uw\frac{\partial^2 w}{\partial z\partial r}\right]\\
&+\lambda_2\left[\begin{array}{c}u^3\frac{\partial^3 w}{\partial r^3}+w^3\frac{\partial^3 w}{\partial z^3}+2u^2\left(\frac{\partial u}{\partial r}\frac{\partial^2 w}{\partial r^2}+\frac{\partial w}{\partial r}\frac{\partial^2 w}{\partial r\partial z}\right)-u^2\left(\frac{\partial w}{\partial r}\frac{\partial^2 u}{\partial r^2}+\frac{\partial w}{\partial z}\frac{\partial^2 w}{\partial r^2}\right)\\+2w^2\frac{\partial u}{\partial z}\frac{\partial^2 w}{\partial r\partial z}+w^2\left(\frac{\partial w}{\partial z}\frac{\partial^2 w}{\partial z^2}-\frac{\partial w}{\partial r}\frac{\partial^2 u}{\partial z^2}\right)+3uw\left(u\frac{\partial^3 w}{\partial r^2\partial z}+w\frac{\partial^3 w}{\partial z^2\partial r}\right)\\+2uw\left(\frac{\partial u}{\partial r}\frac{\partial^2 w}{\partial z\partial r}+\frac{\partial u}{\partial z}\frac{\partial^2 w}{\partial r^2}+\frac{\partial w}{\partial r}\frac{\partial^2 w}{\partial z^2}-\frac{\partial w}{\partial r}\frac{\partial^2 u}{\partial r\partial z}\right)\end{array}\right]\\
&=\nu\left[\frac{\partial^2 w}{\partial r^2}+\frac{1}{r}\frac{\partial w}{\partial r}\right]-\frac{\sigma B_0^2}{\rho}\left[\begin{array}{c}w+\lambda_1 u\frac{\partial w}{\partial r}+\\ \lambda_2\left(w\frac{\partial u}{\partial z}\frac{\partial^2 w}{\partial r^2}-u\frac{\partial w}{\partial z}\frac{\partial^2 w}{\partial r^2}+uw\frac{\partial^2 w}{\partial r\partial z}+u^2\frac{\partial^2 w}{\partial r^2}\right)\end{array}\right].\\
&+\nu\lambda_3\left[\begin{array}{c}u\frac{\partial^3 w}{\partial r^3}+w\frac{\partial^3 w}{\partial r^2\partial z}+\frac{u}{r}\frac{\partial^2 w}{\partial r^2}-\frac{\partial w}{\partial r}\frac{\partial^2 u}{\partial r^2}+\frac{w}{r}\frac{\partial^2 w}{\partial r\partial z}\\-\frac{1}{r}\frac{\partial u}{\partial r}\frac{\partial w}{\partial r}-\frac{1}{r}\frac{\partial w}{\partial r}\frac{\partial w}{\partial z}-\frac{\partial w}{\partial z}\frac{\partial^2 u}{\partial r^2}\end{array}\right]
\end{aligned}
\tag{2}
$$

$$
\begin{aligned}
&u\frac{\partial T}{\partial r}+w\frac{\partial T}{\partial z}-\tau\frac{D_t}{T_\infty}\left[\left(\frac{\partial T}{\partial r}\right)^2+2\lambda_t\left(u\frac{\partial T}{\partial r}\frac{\partial^2 T}{\partial r^2}+w\frac{\partial T}{\partial z}\frac{\partial^2 T}{\partial z^2}\right)\right]\\
&-\tau D_b\left[\frac{\partial C}{\partial r}\frac{\partial T}{\partial r}-\lambda_t\left(u\frac{\partial^2 T}{\partial r^2}\frac{\partial C}{\partial z}+u\frac{\partial^2 C}{\partial r^2}\frac{\partial T}{\partial r}+w\frac{\partial^2 T}{\partial r\partial z}\frac{\partial C}{\partial r}+w\frac{\partial^2 C}{\partial r\partial z}\frac{\partial T}{\partial r}\right)\right]\\
&+\lambda_t\left[u^2\frac{\partial^2 T}{\partial r^2}+w^2\frac{\partial^2 T}{\partial z^2}+2uw\frac{\partial^2 T}{\partial r\partial z}+u\frac{\partial u}{\partial r}\frac{\partial T}{\partial r}+u\frac{\partial w}{\partial r}\frac{\partial T}{\partial z}+w\frac{\partial u}{\partial z}\frac{\partial T}{\partial r}+w\frac{\partial w}{\partial z}\frac{\partial T}{\partial z}\right]\\
&=\alpha_1\left[\frac{1}{r}\frac{\partial}{\partial r}\left(\frac{\partial T}{\partial r}\right)\right]+\frac{Q_0}{\rho c_p}\left[(T-T_\infty)+\lambda_t\left(u\frac{\partial T}{\partial r}+w\frac{\partial T}{\partial z}\right)\right]\\
&+\frac{\sigma B_0^2}{\rho c_p}\left[w^2+\lambda_t\left(2w^2\frac{\partial w}{\partial z}+2uw\frac{\partial u}{\partial r}\right)\right],
\end{aligned}
\tag{3}
$$

with boundary conditions

$$
w=w_s=\frac{U_0 z}{l},\ u=0,\ T=T_w,\ C=C_w \text{ at } r=R, \tag{5}
$$

$$
w\to 0,\ \frac{\partial w}{\partial r}\to 0,\ T\to T_\infty,\ C\to C_\infty \text{ as } r\to\infty. \tag{6}
$$

Here (u,w) are the velocity components in r and z directions respectively, ν the kinematics viscosity, λ_1 the relaxation time, λ_2 the material parameter of Burgers fluid, λ_3 $(\leq\lambda_1)$ the retardation time, (T,C) the liquid temperature and concentration respectively, (T_∞,C_∞) the ambient temperature and the ambient concentration, D_B the diffusion coefficient and $\alpha_1=\left(\frac{k}{(\rho c)_f}\right)$ the thermal diffusivity, in which (ρ_f,c_f) are the density of liquid and specific heat respectively, and k the thermal conductivity of the liquid.

Introducing the following dimensionless transformations

$$
\begin{aligned}
u=-\frac{R}{r}\sqrt{\frac{U_0\nu}{l}}f(\eta),\ w=\frac{U_0 z}{l}f'(\eta),\ \theta(\eta)=\frac{T-T_\infty}{T_w-T_\infty},\\
\times\phi(\eta)=\frac{C-C_\infty}{C_w-C_\infty},\ \eta=\sqrt{\frac{U_0}{\nu l}}\left(\frac{r^2-R^2}{2R}\right).
\end{aligned}
\tag{7}
$$

By employing above conversions, equation (1) is satisfied automatically and equations (2)–(4) yield

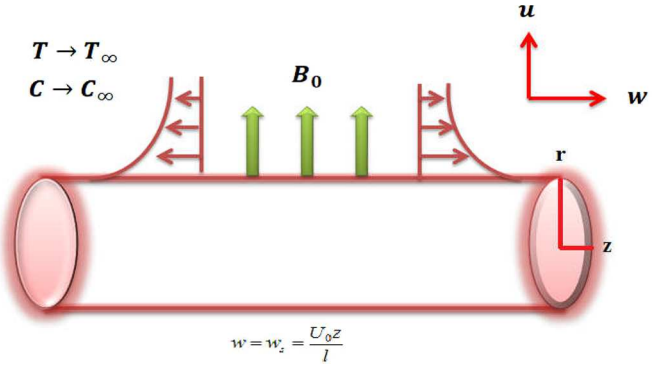

Fig. 1. Flow configuration with coordinate axes.

$$
\begin{aligned}
&(1+2\alpha\eta)^2\beta_1\left[2ff'f''-f^2f'''\right]-(1+2\alpha\eta)\alpha\beta_1 f^2 f''\\
&+(1+2\alpha\eta)^3 f'''+(1+2\alpha\eta)\alpha\beta_2\left[3f^2f'f''+f^3f'''\right]\\
&+(1+2\alpha\eta)^2\left[2\alpha f''+ff''-(f')^2\right]\\
&-(1+2\alpha\eta)^2\beta_2\left[3f^2(f'')^2+2f(f')^2f''-f^3f^{iv}\right]\\
&-4\alpha^2\beta_2 f'''f''+(1+2\alpha\eta)^3\beta_3\left[(f'')^2-ff^{iv}\right]\\
&-4\alpha\beta_3(1+2\alpha\eta)^2 ff'''\\
&-(1+2\alpha\eta)^2 M^2\left[\beta_2 ff'''-\beta_1 ff''+f'\right]=0,
\end{aligned}
\tag{8}
$$

Table 1. A comparison table for $-f''(0)$ for distinct scales of β_1 when $\alpha = \beta_2 = \beta_3 = M = 0$.

β_1	Abel et al. [33]	Irfan et al. [34]	Present study
0.0	1.00000	1.0000000	1.0000000
0.2	1.051948	1.0518890	1.0518799
0.4	1.101850	1.1019035	1.1019100
0.6	1.150163	1.1501374	1.1501368
0.8	1.196692	1.1967114	1.1967121
1.2	1.285257	1.2853630	1.2853578

Table 2. A comparison table for $-f''(0)$ for distinct scales of M when $\alpha = \beta_1 = \beta_2 = \beta_3 = 0$.

M	Fathizadeh et al. [35]	Ahmed et al. [36]	Present study
0.5		1.224745	1.224739
1.0	1.41421	1.414213	1.414211
1.5			1.581028
2.0			1.731939
5.0	2.44948	2.449474	2.449396

$$
\begin{aligned}
&(1+2\alpha\eta)\,\theta'' + 2\alpha\theta' + \Pr\left[\theta' f - \beta_t(f' f\theta' + f^2\theta'')\right] \\
&+\Pr\delta\left[\theta + \beta_t(f\theta')\right] + \Pr N_b\left[\phi^{'}\theta^{'}\,(1+2\alpha\eta)\right. \\
&\left.-\beta_t\{2\alpha f\theta'\phi' + (1+2\alpha\eta)\,(f\theta''\phi' + f\theta'\phi'')\}\right] \\
&\Pr N_t\left[\theta^{'^2}\,(1+2\alpha\eta) - 2\beta_t\{(1+2\alpha\eta)\,f\theta'\theta'' + \alpha f\theta^{'^2}\}\right] \\
&+2\Pr MEc\left[f^{'^2} + \beta_1(f^{'^3} - ff'f'')\right] = 0, \qquad (9)
\end{aligned}
$$

$$
\begin{aligned}
&(1+2\alpha\eta)\,\phi'' + 2\alpha\phi' + Sc[f\phi' - \beta_c(f' f\phi' + f^2\phi'')] \\
&-Sck\left[\phi + \beta_c(f\phi')\right] + \left(\frac{N_t}{N_b}\right)\left[(1+2\alpha\eta)\theta^{''}\right. \\
&\left.-\beta_c(f\theta''' - 4\alpha f\theta'')\right] = 0, \qquad (10)
\end{aligned}
$$

and transformed boundary conditions are as follows

$$f = 0,\ f' = 1,\ \theta = 1,\ \phi = 1 \text{ at } \eta = 0, \qquad (11)$$

$$f' \to 0,\ f'' \to 0,\ \theta \to 0,\ \phi \to 0 \text{ as } \eta \to \infty. \qquad (12)$$

Here, $M = \left(\frac{\sigma l B_0^2}{\rho_f U_0}\right)^{1/2}$ is the magnetic parameter, $\alpha\left(= \frac{1}{R}\sqrt{\frac{\nu l}{U_0}}\right)$ the curvature parameter, $\beta_1\left(= \lambda_1\frac{U_0}{l}\right)$ the fluid relaxation time constant, $\beta_3\left(= \lambda_3\frac{U_0}{l}\right)$ the fluid retardation time constant, $\beta_2\left(= \lambda_2\left(\frac{U_0}{l}\right)^2\right)$ the Burgers fluid parameter, $\Pr\left(= \frac{\nu}{\alpha_1}\right)$ the Prandtl number, $Ec\left(= \frac{w^2}{c_p(T_w - T_\infty)}\right)$ the Eckert number, $\delta\left(= \frac{lQ_0}{U_0(\rho c_p)}\right)$ the heat source/sink parameter, $Sc\left(= \frac{\nu}{D_B}\right)$ the Schmidt number, $k_1\left(= \frac{k_c l}{U_0}\right)$ the chemical reaction parameter, $N_t\left(= \frac{\tau D_T(T_w - T_\infty)}{\nu T_\infty}\right)$ the thermophoresis parameter and $N_b\left(= \frac{\tau D_B(C_w - C_\infty)}{\nu}\right)$ the Brownian motion parameter.

3 Validation of Homotopic results

We computed several values of $-f''(0)$ for different magnitudes of β_1 and M in Tables 1 and 2 respectively. These values are compared with already published studies and we find that our values are in good agreement with these studies which clarify that the used homotopic approach is valid.

4 Solution methodology of HAM

In this section the principle of homotopy analysis method (HAM) is briefly discussed. In this technique the initial guesses and linear operators are required to initiate the process. Here, (f_0, θ_0, ϕ_0) are chosen as initial guesses while, $(\pounds_f, \pounds_\theta, \pounds_\phi)$ are adopted as linear operators which are defined below

$$\phi_0(\eta) = e^{-\eta},\ \theta_0(\eta) = e^{-\eta},\ f_0(\eta) = 1 - e^{-\eta}, \qquad (13)$$

$$\pounds_\phi[\phi(\eta)] = \phi'' - \phi,\ \pounds_\theta[\theta(\eta)] = \theta'' - \theta,\ \pounds_f[f(\eta) = f''' - f', \qquad (14)$$

with following properties

$$
\begin{aligned}
&\pounds_\phi[B_6^* e^{\eta} + B_7^* e^{-\eta}] = 0,\ \pounds_\theta[B_4^* e^{\eta} + B_5^* e^{-\eta}] = 0, \\
&\pounds_f[B_1^* + B_2^* e^{\eta} + B_3^* e^{-\eta}] = 0, \qquad (15)
\end{aligned}
$$

where $B_i^*(i = 1-7)$ denote constants.

The zeroth order deformation problem is defined below

$$\pounds_f[f(\eta;c) - f_0(\eta)]\,(1-c) = c\acute{N}_f\hbar_f[\widetilde{f}(\eta;c)], \qquad (16)$$

$$\pounds_\theta[\theta(\eta;c) - \theta_0(\eta)]\,(1-c) = c\acute{N}_\theta\hbar_\theta[\widetilde{f}(\eta;c), \widetilde{\theta}(\eta;c), \widetilde{\phi}(\eta;c)], \qquad (17)$$

$$\pounds_\phi[\phi(\eta;c) - \phi_0(\eta)]\,(1-c) = c\acute{N}_\phi\hbar_\phi[\widetilde{f}(\eta;c), \widetilde{\theta}(\eta;c), \widetilde{\phi}(\eta;c)], \qquad (18)$$

$$
\begin{aligned}
&\phi(0;c) = 1,\ \theta(0;c) = 1,\ \widetilde{f}(0;c) = 0,\ \frac{\partial\widetilde{f}(0;c)}{\partial\eta} = 1, \\
&\phi(\infty;c) = 0,\ \theta(\infty;c) = 0,\ \frac{\partial\widetilde{f}(\infty;c)}{\partial\eta} = 0,\ \frac{\partial^2\widetilde{f}(\infty;c)}{\partial\eta^2} = 0, \qquad (19)
\end{aligned}
$$

with nonlinear operators

$$\acute{N}_f[\widetilde{f}(\eta;c)] = (1+2\alpha\eta)^2\,\beta_1\left[2\widetilde{f}\frac{\partial\widetilde{f}}{\partial\eta}\frac{\partial^2\widetilde{f}}{\partial\eta^2} - \widetilde{f}^2\frac{\partial^3\widetilde{f}}{\partial\eta^3}\right]$$
$$+(1+2\alpha\eta)^3\,\frac{\partial^3\widetilde{f}}{\partial\eta^3} - (1+2\alpha\eta)^2\,\beta_2\left[2\widetilde{f}\left(\frac{\partial\widetilde{f}}{\partial\eta}\right)^2\frac{\partial^2\widetilde{f}}{\partial\eta^2}\right.$$
$$\left.-\widetilde{f}^3\frac{\partial^4\widetilde{f}}{\partial\eta^4} + 3\widetilde{f}^2\left(\frac{\partial^2\widetilde{f}}{\partial\eta^2}\right)^2\right] - (1+2\alpha\eta)\,\alpha\beta_1\widetilde{f}^2\frac{\partial^2\widetilde{f}}{\partial\eta^2}$$
$$+(1+2\alpha\eta)\,\alpha\beta_2\left[\widetilde{f}^3\frac{\partial^3\widetilde{f}}{\partial\eta^3} + 3\widetilde{f}^2\frac{\partial\widetilde{f}}{\partial\eta}\frac{\partial^2\widetilde{f}}{\partial\eta^2}\right]$$
$$+(1+2\alpha\eta)^2\left[\widetilde{f}\frac{\partial^2\widetilde{f}}{\partial\eta^2} - \left(\frac{\partial\widetilde{f}}{\partial\eta}\right)^2 + 2\alpha\frac{\partial^2\widetilde{f}}{\partial\eta^2}\right]$$
$$-4\,(1+2\alpha\eta)^2\,\alpha\beta_3\widetilde{f}\frac{\partial^3\widetilde{f}}{\partial\eta^3} - 4\alpha^2\beta_2\frac{\partial^3\widetilde{f}}{\partial\eta^3}\frac{\partial^2\widetilde{f}}{\partial\eta^2}$$
$$+(1+2\alpha\eta)^3\,\beta_3\left[\left(\frac{\partial^2\widetilde{f}}{\partial\eta^2}\right)^2 - \widetilde{f}\frac{\partial^4\widetilde{f}}{\partial\eta^4}\right]$$
$$-(1+2\alpha\eta)^2\,M^2\left[\frac{\partial\widetilde{f}}{\partial\eta} + \beta_2\widetilde{f}\frac{\partial^3\widetilde{f}}{\partial\eta^3} - \beta_1\widetilde{f}\frac{\partial^2\widetilde{f}}{\partial\eta^2}\right], \qquad (20)$$

$$\acute{N}_\theta[\widetilde{f}(\eta;c),\widetilde{\theta}(\eta;c),\widetilde{\phi}(\eta;c)] = (1+2\alpha\eta)\,\frac{\partial^2\widetilde{\theta}}{\partial\eta^2}$$
$$+\Pr\left[\frac{\partial\widetilde{\theta}}{\partial\eta}\widetilde{f} - \beta_t\left(\widetilde{f}\frac{\partial\widetilde{\theta}}{\partial\eta}\frac{\partial\widetilde{f}}{\partial\eta} + \widetilde{f}^2\frac{\partial^2\widetilde{\theta}}{\partial\eta^2}\right)\right]$$
$$+\Pr N_b\left[(1+2\alpha\eta)\,\frac{\partial\widetilde{\phi}}{\partial\eta}\frac{\partial\widetilde{\theta}}{\partial\eta} - \beta_t\left\{2\alpha\widetilde{f}\frac{\partial\widetilde{\theta}}{\partial\eta}\frac{\partial\widetilde{\phi}}{\partial\eta}\right.\right.$$
$$\left.\left.+(1+2\alpha\eta)\left(\widetilde{f}\frac{\partial^2\widetilde{\theta}}{\partial\eta^2}\frac{\partial\widetilde{\phi}}{\partial\eta} + \widetilde{f}\frac{\partial\widetilde{\theta}}{\partial\eta}\frac{\partial^2\widetilde{\phi}}{\partial\eta^2}\right)\right\}\right]$$
$$+\Pr\delta\left[\widetilde{\theta} + \beta_t\widetilde{f}\frac{\partial\widetilde{\theta}}{\partial\eta}\right] + \Pr N_t\left[(1+2\alpha\eta)\left(\frac{\partial\widetilde{\theta}}{\partial\eta}\right)^2\right.$$
$$\left.-2\beta_t\left\{(1+2\alpha\eta)\,\widetilde{f}\frac{\partial\widetilde{\theta}}{\partial\eta}\frac{\partial^2\widetilde{\theta}}{\partial\eta^2} + \alpha\widetilde{f}\left(\frac{\partial\widetilde{\theta}}{\partial\eta}\right)^2\right\}\right]$$
$$+2\alpha\frac{\partial\widetilde{\theta}}{\partial\eta} + 2\Pr MEc\left[\left(\frac{\partial\widetilde{f}}{\partial\eta}\right)^2 + \beta_1(\left(\frac{\partial\widetilde{f}}{\partial\eta}\right)^3\right.$$
$$\left.-\widetilde{f}\frac{\partial\widetilde{f}}{\partial\eta}\frac{\partial^2\widetilde{f}}{\partial\eta^2})\right] = 0, \qquad (21)$$

$$\acute{N}_\phi[\widetilde{f}(\eta;c),\widetilde{\theta}(\eta;c),\widetilde{\phi}(\eta;c)] = (1+2\alpha\eta)\,\frac{\partial^2\widetilde{\phi}}{\partial\eta^2}$$
$$+2\alpha\frac{\partial\widetilde{\phi}}{\partial\eta} - Sck\left(\widetilde{\phi} + \beta_c\widetilde{f}\frac{\partial\widetilde{\phi}}{\partial\eta}\right)$$
$$+\left(\frac{N_t}{N_b}\right)\left[(1+2\alpha\eta)\frac{\partial^2\widetilde{\theta}}{\partial\eta^2} - \beta_c\left(\widetilde{f}\frac{\partial^3\widetilde{\theta}}{\partial\eta^3} - 4\alpha\widetilde{f}\frac{\partial^2\widetilde{\theta}}{\partial\eta^2}\right)\right]$$
$$+Sc\left[\widetilde{f}\frac{\partial\widetilde{\phi}}{\partial\eta} - \beta_c\left(\widetilde{f}\frac{\partial\widetilde{f}}{\partial\eta}\frac{\partial\widetilde{\phi}}{\partial\eta} + \widetilde{f}^2\frac{\partial^2\widetilde{\phi}}{\partial\eta^2}\right)\right] = 0. \qquad (22)$$

For $c=0$ and $c=1$ respectively, we get

$$\widetilde{f}(\eta;0) = f_0(\eta),\ \widetilde{\theta}(\eta;0) = \theta_0(\eta),\ \widetilde{\phi}(\eta;0) = \phi_0(\eta), \qquad (23)$$

$$\widetilde{f}(\eta;1) = f(\eta),\ \widetilde{\theta}(\eta;1) = \theta(\eta),\ \widetilde{\phi}(\eta;1) = \phi(\eta). \qquad (24)$$

Note that when c changes from 0 to 1 then $f_0(\eta), \theta_0(\eta)$ and $\phi_0(\eta)$ approach $f(\eta)$, $\theta(\eta)$ and $\phi(\eta)$ respectively. Taylor series enables us to have

$$\widetilde{f}(\eta;c) = f_0(\eta) + \sum_{m=1}^{\infty} c^m f_m(\eta),\ f_m(\eta) = \frac{1}{m!}\frac{\partial^m\widetilde{f}(\eta;c)}{\partial\eta^m}\text{at } c=0, \qquad (25)$$

$$\widetilde{\theta}(\eta;c) = \theta_0(\eta) + \sum_{m=1}^{\infty} c^m \theta_m(\eta),\ \theta_m(\eta) = \frac{1}{m!}\frac{\partial^m\widetilde{\theta}(\eta;c)}{\partial\eta^m}\text{at } c=0, \qquad (26)$$

$$\widetilde{\phi}(\eta;c) = \phi_0(\eta) + \sum_{m=1}^{\infty} c^m \phi_m(\eta),\ \phi_m(\eta) = \frac{1}{m!}\frac{\partial^m\widetilde{\phi}(\eta;c)}{\partial\eta^m}\text{at } c=0. \qquad (27)$$

Here, $\hbar_f$, $\hbar_\theta$ and $\hbar_\phi$ are auxiliary parameters which control the convergence regarding equations (25)–(27). By selection of appropriate values of $\hbar_f, \hbar_\theta$ and $\hbar_\phi$ equations (25)–(27) converge at $c=1$. Hence we get

$$\widetilde{f}(\eta;c) = f_0(\eta) + \sum_{m=1}^{\infty} f_m(\eta),$$
$$\widetilde{\theta}(\eta;c) = \theta_0(\eta) + \sum_{m=1}^{\infty} \theta_m(\eta),$$
$$\widetilde{\phi}(\eta;c) = \phi_0(\eta) + \sum_{m=1}^{\infty} \phi_m(\eta).$$

The mth order deformation problems are defined as follows

$$\pounds_f[f_m(\eta) - \chi_m f_{m-1}(\eta)] = \hbar_f\acute{R}_f^m(\eta), \qquad (28)$$

$$\pounds_f[\theta_m(\eta) - \chi_m\theta_{m-1}(\eta)] = \hbar_\theta\acute{R}_\theta^m(\eta), \qquad (29)$$

$$\pounds_f[\phi_m(\eta) - \chi_m\phi_{m-1}(\eta)] = \hbar_\phi \acute{R}^m_\phi(\eta), \tag{30}$$

$$\phi_m(0) = 1,\ \theta_m(0) = 1,\ f_m(0) = 0,\ \frac{\partial f_m(\eta)}{\partial\eta}|_{\eta=0} = 1,$$
$$\phi_m(\infty) = 0,\ \theta_m(\infty) = 0,\ \frac{\partial f_m(\eta)}{\partial\eta}|_{\eta=\infty} = 0,\ \frac{\partial^2 f_m(\eta)}{\partial\eta^2}|_{\eta=\infty} = 0, \tag{31}$$

$$\begin{aligned}
\acute{R}^m_f(\eta) &= (1+2\alpha\eta)^3 f'''_{m-1} - (1+2\alpha\eta)^2 \sum_{k=0}^{m-1} f'_{m-1-k} f'_k \\
&+(1+2\alpha\eta)^2 \sum_{k=0}^{m-1} f_{m-1-k} f''_k \\
&+2(1+2\alpha\eta)^2\beta_1 \sum_{k=0}^{m-1} f_{m-1-k} \sum_{l=0}^{k} f'_{k-l} f''_l \\
&+\beta_2(1+2\alpha\eta)^2 \sum_{l=0}^{k} f_{k-l} \sum_{k=0}^{m-1} f_{m-1-k} \sum_{i=0}^{l} f_{l-i} f^{iv}_i \\
&-\beta_1(1+2\alpha\eta)^2 \sum_{l=0}^{k} f_{k-l} f'''_l \sum_{k=0}^{m-1} f_{m-1-k} \\
&-2(1+2\alpha\eta)^2\beta_2 \sum_{l=0}^{k} f'_{k-l} \sum_{k=0}^{m-1} f_{m-1-k} \sum_{i=0}^{l} f'_{l-i} f''_i \\
&-3(1+2\alpha\eta)^2\beta_2 \sum_{k=0}^{m-1} f_{m-1-k} \sum_{l=0}^{k} f_{k-l} \sum_{i=0}^{l} f''_{l-i} f''_i \\
&+(1+2\alpha\eta)\alpha\beta_2 \sum_{k=0}^{m-1} f'_{m-1-k} \sum_{l=0}^{k} f_{k-l} \sum_{i=0}^{l} f_{l-i} f''_i \\
&(1+2\alpha\eta)^3\beta_3 \sum_{k=0}^{m-1} f''_{m-1-k} f''_k \\
&-(1+2\alpha\eta)^3\beta_3 \sum_{k=0}^{m-1} f_{m-1-k} f^{iv}_k \\
&+2\alpha(1+2\alpha\eta)^2 f''_{m-1} \\
&(1+2\alpha\eta)\alpha\beta_2 \sum_{k=0}^{m-1} f_{m-1-k} \sum_{l=0}^{k} f_{k-l} \sum_{i=0}^{l} f_{l-i} f'''_i \\
&-4\alpha\beta_3(1+2\alpha\eta)^2 \sum_{k=0}^{m-1} f_{m-1-k} f'''_k \\
&+(1+2\alpha\eta)^2 M^2\beta_2 \sum_{k=0}^{m-1} f_{m-1-k} f''''_k \\
&-(1+2\alpha\eta)\alpha\beta_1 \sum_{k=0}^{m-1} f_{m-1-k} \sum_{l=0}^{k} f_{k-l} f''_l \\
&-4\alpha^2\beta_2 \sum_{k=0}^{m-1} f''_{m-1-k} f'''_k \\
&-(1+2\alpha\eta)^2 M^2 f'_{m-1} \\
&+(1+2\alpha\eta)^2 M^2\beta_1 \sum_{k=0}^{m-1} f_{m-1-k} f''_k,
\end{aligned} \tag{32}$$

$$\begin{aligned}
\acute{R}^m_\theta(\eta) &= (1+2\alpha\eta)\theta''_{m-1} + 2\alpha\theta'_{m-1} \\
&-\Pr\beta_t \sum_{k=0}^{m-1} f_{m-1-k} \sum_{l=0}^{k} f'_{k-l}\theta'_l + \Pr\beta_t \sum_{k=0}^{m-1} f_{m-1-k} \sum_{l=0}^{k} f_{k-l}\theta''_l \\
&+2\Pr MEc \sum_{k=0}^{m-1} f'_{m-1-k} f'_k \\
&-2\Pr MEc\beta_1 \sum_{k=0}^{m-1} f_{m-1-k} \sum_{l=0}^{k} f'_{k-l} f''_l \\
&-2\alpha\Pr N_b\beta_t \sum_{k=0}^{m-1} f_{m-1-k} \sum_{l=0}^{k} \theta'_{k-l}\phi'_l \\
&+\Pr \sum_{k=0}^{m-1} f_{m-1-k}\theta'_k + \Pr\delta\theta_{m-1} + \Pr\delta\beta_t \sum_{k=0}^{m-1} f_{m-1-k}\theta'_k \\
&+(1+2\alpha\eta)\Pr N_b \sum_{k=0}^{m-1} \theta'_{m-1-k}\phi'_k \\
&+(1+2\alpha\eta)\Pr N_b\beta_t \sum_{k=0}^{m-1} f_{m-1-k} \sum_{l=0}^{k} \phi'_{k-l}\theta''_l \\
&+(1+2\alpha\eta)\Pr N_b\beta_t \sum_{k=0}^{m-1} f_{m-1-k} \sum_{l=0}^{k} \theta'_{k-l}\phi''_l \\
&+(1+2\alpha\eta)\Pr N_t \sum_{k=0}^{m-1} \theta'_{m-1-k}\theta'_k \\
&-2\beta_t(1+2\alpha\eta)\Pr N_t \sum_{k=0}^{m-1} f_{m-1-k} \sum_{l=0}^{k} \theta'_{k-l}\theta''_l \\
&-2\alpha\beta_t\Pr N_t \sum_{k=0}^{m-1} f_{m-1-k} \sum_{l=0}^{k} \theta'_{k-l}\theta'_l \\
&+2\Pr MEc\beta_1 \sum_{k=0}^{m-1} f'_{m-1-k} \sum_{l=0}^{k} f'_{k-l} f'_l,
\end{aligned} \tag{33}$$

$$\begin{aligned}
\acute{R}^m_\phi(\eta) &= (1+2\alpha\eta)\phi''_{m-1} + 2\alpha\phi'_{m-1} + Sc \sum_{k=0}^{m-1} f_{m-1-k}\phi'_k \\
&-Sc\beta_c \sum_{k=0}^{m-1} f_{m-1-k} \sum_{l=0}^{k} f'_{k-l}\phi'_l \\
&-Sc\beta_c \sum_{k=0}^{m-1} f_{m-1-k} \sum_{l=0}^{k} f_{k-l}\phi''_l - Sck\phi_{m-1} \\
&-Sck\beta_c \sum_{k=0}^{m-1} f_{m-1-k}\phi'_k + (1+2\alpha\eta)\left(\frac{N_t}{N_b}\right)\theta''_{m-1} \\
&-\beta_c\left(\frac{N_t}{N_b}\right)\sum_{k=0}^{m-1} f_{m-1-k}\theta'''_k + 4\alpha\beta_c\left(\frac{N_t}{N_b}\right)\sum_{k=0}^{m-1} f_{m-1-k}\theta''_k,
\end{aligned} \tag{34}$$

and we have

$$\chi_m = \begin{pmatrix} 0, & m \le 1 \\ 1, & m > 1 \end{pmatrix}.$$

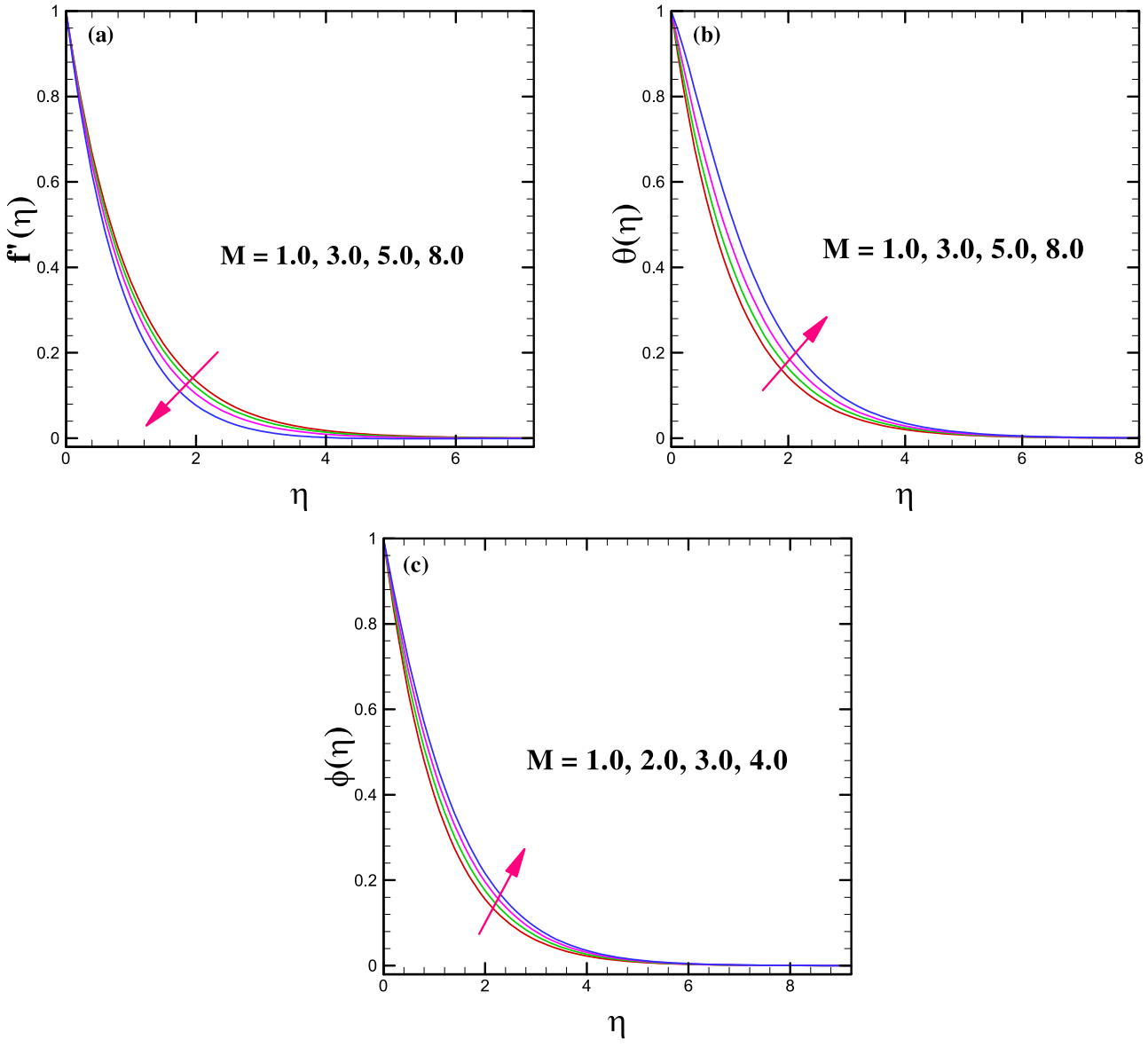

Fig. 2. (a-c): Impact of M on flow, temperature and concentration fields.

Following relations are representing the general solutions.

$$f_m(\eta) = B_1^* + B_2^* e^{\eta} + B_3^* e^{-\eta} + f_m^*(\eta), \tag{35}$$

$$\theta_m(\eta) = B_4^* + B_5^* e^{-\eta} + \theta_m^*(\eta), \tag{36}$$

$$\phi_m(\eta) = B_6^* + B_7^* e^{-\eta} + \phi_m^*(\eta), \tag{37}$$

whereas the constants B_j $(j = 1$ to $7)$ are achieved by utilizing the boundary conditions $35 - 37$.i.e,

$$B_2^* = B_4^* = B_6^* = 0,\ B_3^* = \frac{\partial f_m^*(\eta)}{\partial \eta}|_{\eta=0} = 0,$$
$$B_1^* = -B_3^* - f_m^*(0),\ B_5^* = -\theta_m^*(0),\ B_7^* = -\phi_m^*(0). \tag{38}$$

5 Analysis of results

We employed homotopy analysis method (HAM) to investigate the behaviors of physical parameters occur in ODES (8−10) with associated boundary conditions (11) and (12). We checked the impact of involved parameters on velocity $f'(\eta)$, thermal $\theta(\eta)$ and solutal $\phi(\eta)$ distributions of Burgers nanofluid. The impact of physical parameters is depicted in the form of graphs and discussed with suitable arguments. Moreover fixed values are assigned to leading dimensionless parameters such as $\alpha = 0.25$, $\beta_1 = 0.75$, $\beta_2 = 0.3$, $\beta_3 = 0.5$, $N_t = 0.6$, $N_b = 0.4$, $\beta_t = 0.5$, $\beta_c = 0.4$, $Ec = 1.5$, $M = 2.0$, $\delta = 1.5$, $\Pr = 5.0$, $k_1 = 0.7$, $Sc = 4.0$, during the entire computations.

Figures 2a–2c expose the features of thermal curves for distinct scales of magnetic parameter. It is analyzed that

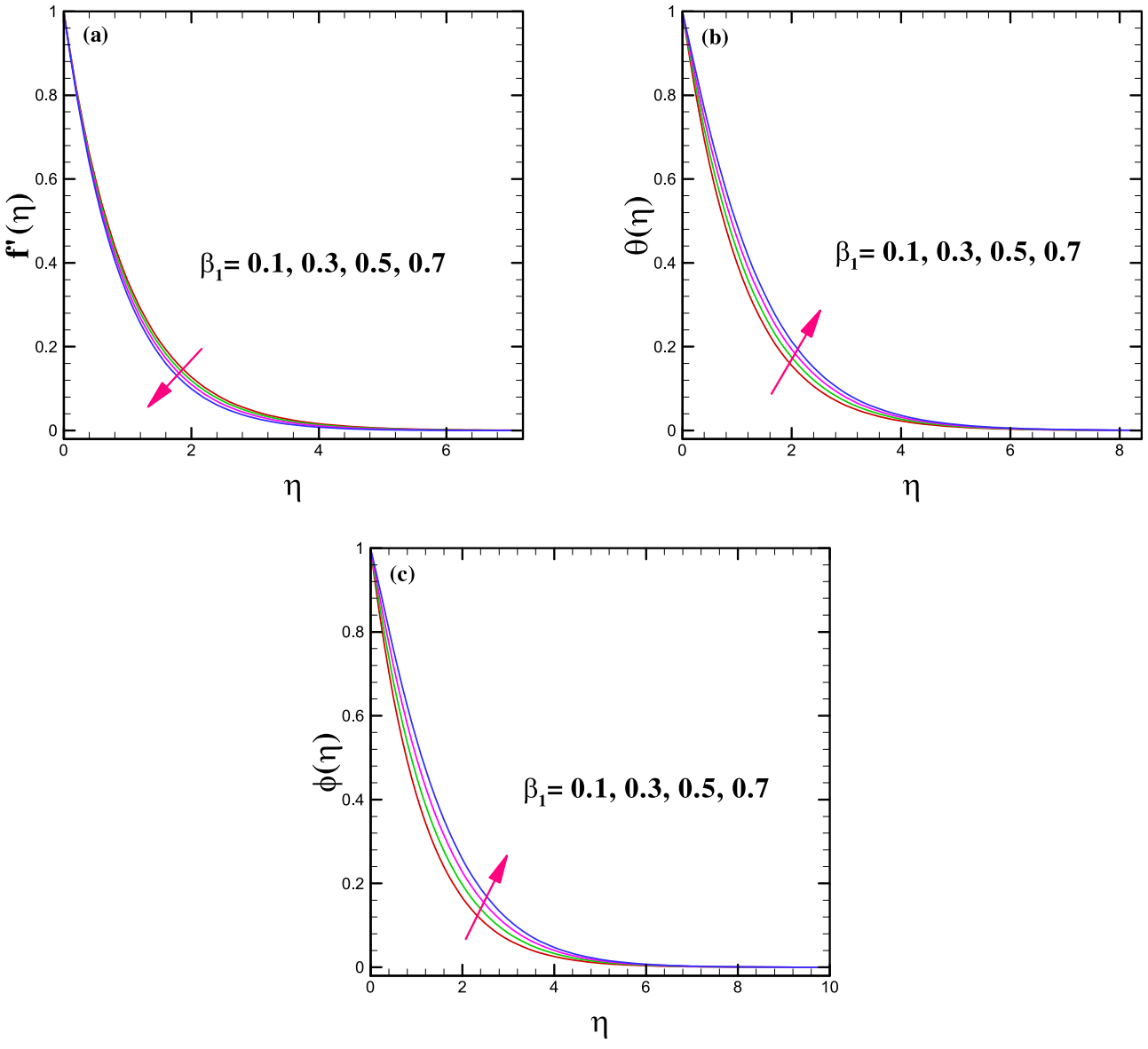

Fig. 3. (a-c): Impact of β_1 on flow, temperature and concentration fields.

the flow curves of Burgers nano liquid decline for higher intensity of magnetic force constant while in contrast of this the thermal and solutal curves of nanofluid depict mounting trend for intensifying magnitude of magnetic force variable. These behaviors are as expected because, larger scales of magnetic force constant lead to produce the escalating amount of Lorentz force which opposes the fluid motion and enhance the temperature and solutal distributions of fluid. Growing amount of Lorentz force generates friction due to which it happens. The influence of relaxation time constant (β_1) towards flow, thermal and solutal distributions is illustrated through Figures 3a–3c. It is depicted that the motion of the fluid retards while heat transport and mass diffusion augments for higher values of β_1. Physical justification of these behaviors is that, the larger relaxation time corresponds to rise the resistance between fluid particles and therefore flow profile of fluid depreciates while thermal and solutal energy transport enhance. The importance of Burgers fluid parameter (β_2) for motion, temperature and concentration distributions of Burgers fluid is represented in Figures 4a–4c. These figures indicate that the motion of the nanofluid depreciates while the thermal and solutal energy transport curves show ascending trend for higher amount of (β_2). The significance of retardation time parameter (β_3) on flow, thermal and solutal lines is previewed in Figures 5a–5c. Through these graphs, it is visualized that the higher magnitude of retardation time constant leads to speed up the motion of the fluid while energy of the system depreciates. Physically, the time taken for the building of shear stress in the liquid is termed as retardation time. Hence, larger retardation time corresponds to accelerate the fluid flow and therefore fluid motion drives up. Additionally, the elasticity of the liquid also boosts up

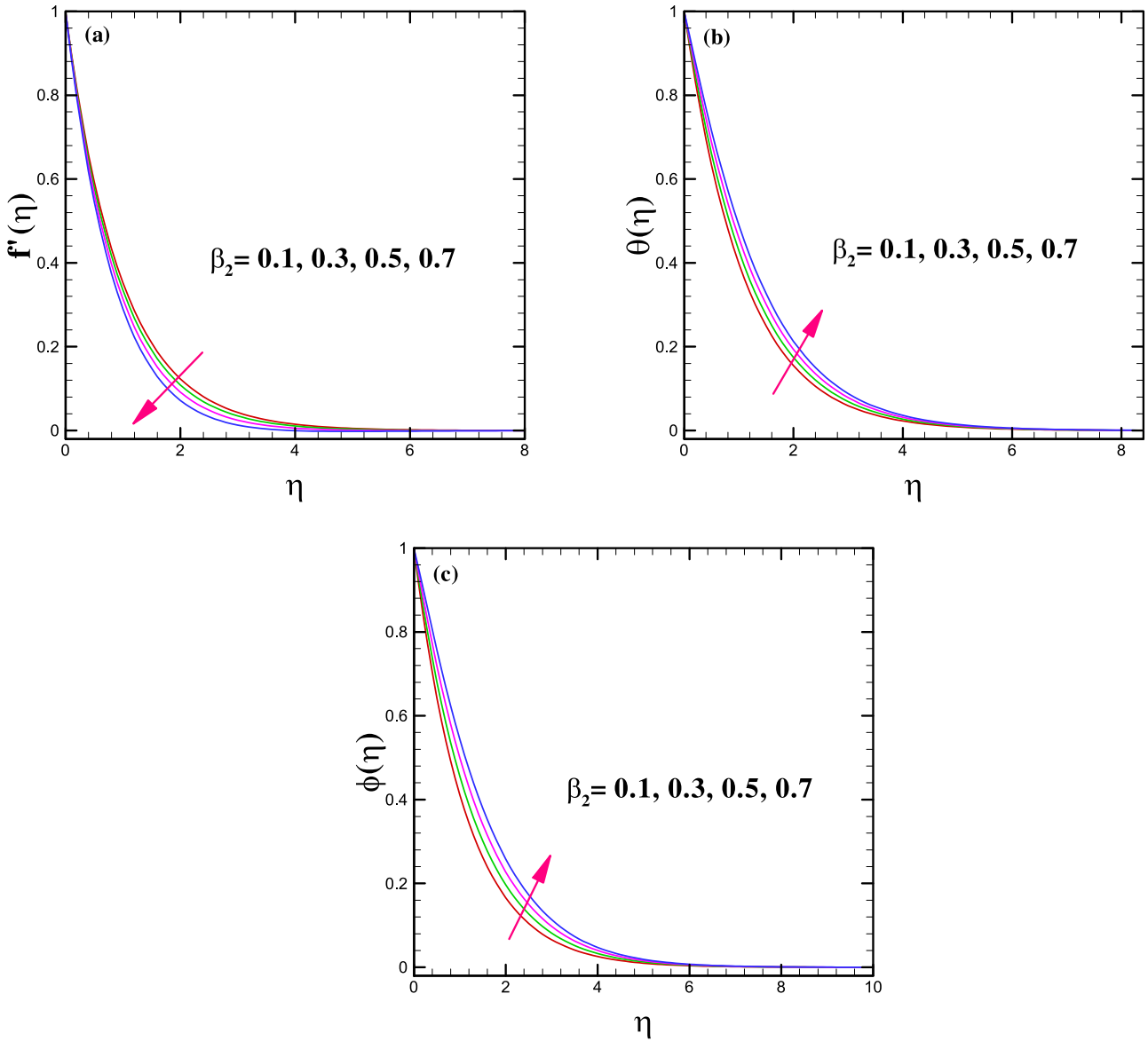

Fig. 4. (a-c): Impact of β_2 on flow, thermal and solutal profiles.

for varying scales of retardation time due to which collision between fluid elements diminishes and therefore the heat flow as well as the mass diffusion process slow down. The role of thermal and solutal relaxation time constants (β_t, β_c) on temperature and concentration distributions, respectively, is demonstrated through Figures 6a, 6b. It is observed that both the thermal and concentration curves of Burgers nanofluid deteriorate for magnifying effects of thermal and solutal relaxation time constants. These results are according to reality that, further time requires for transportation of heat waves to nearby particles of liquid when thermal relaxation time rises therefore the temperature curves of nanofluid weaken. Moreover, mass diffusion needs additional time by intensifying the values of solutal relaxation time constant and consequently, the diminution in the nano particles volume fraction profile is assured. Figure 7 irradiates the impact of Eckert number (Ec) on thermal distribution of reactive Burgers nanofluid. It is analysed that due to accretion in the Eckert number the magnitude of kinetic energy magnifies throughout in the system and this situation leads to improve the transport of temperature in the flow and hence thermal curves of Burgers fluid seem to be strengthen in the graph. Furthermore, Figures 8a, 8b are depicted to highlight the significance of thermophoretic force constant (N_t) on temperature and solutal distribution of nanofluid. These plots demonstrate that the thermal as well as nano particles concentration distributions of nanofluid both build up for amplifying magnitudes of thermophoresis constant. The values taken for N_t are mentioned in graphs. In thermophoresis process, because of change in temperature the fluid particles start moving from warmer to chiller zone and hence the thermal energy and concentration of the system boost up as

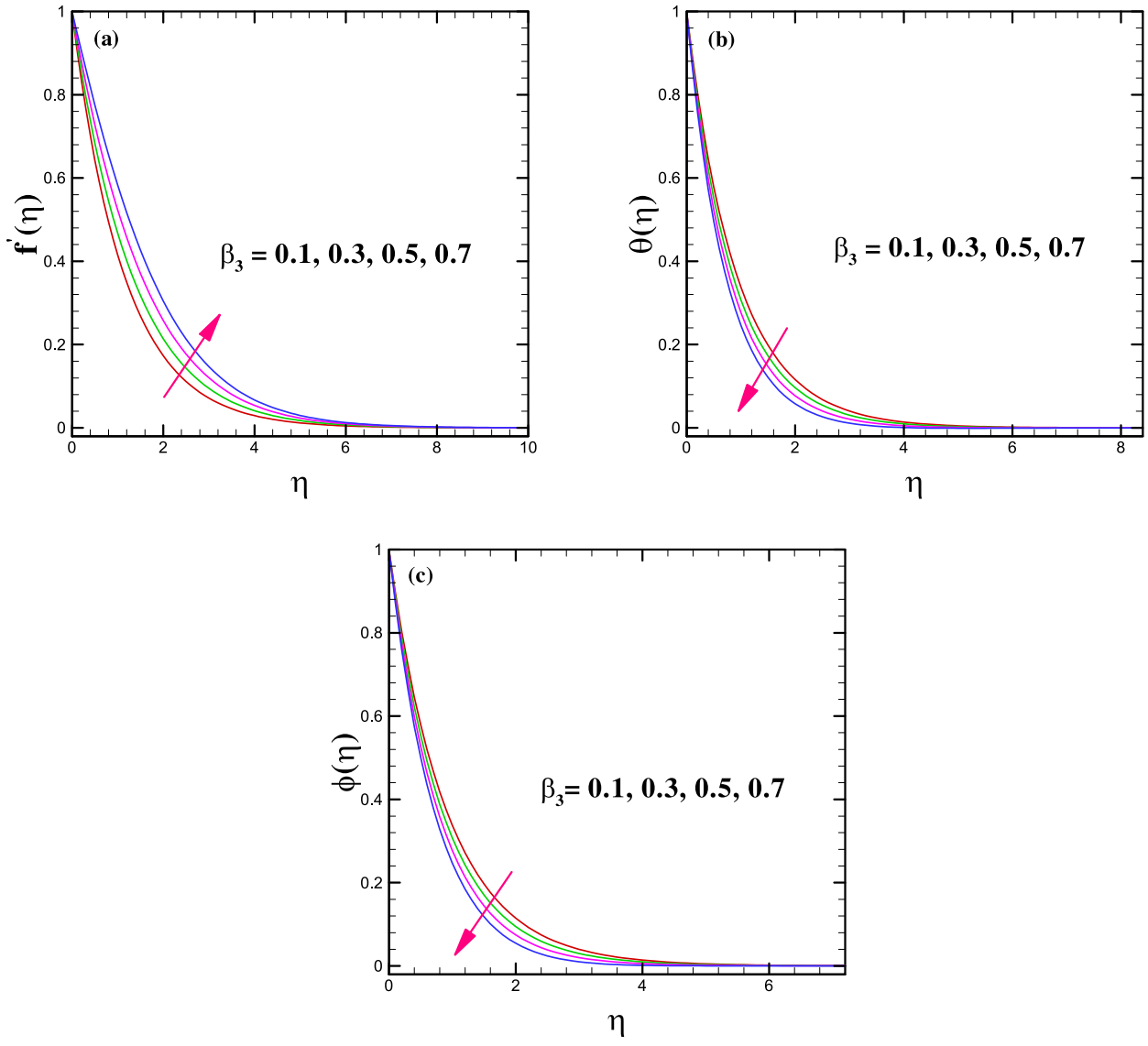

Fig. 5. (a-c): Impact of β_3 on flow, thermal and solutal profiles.

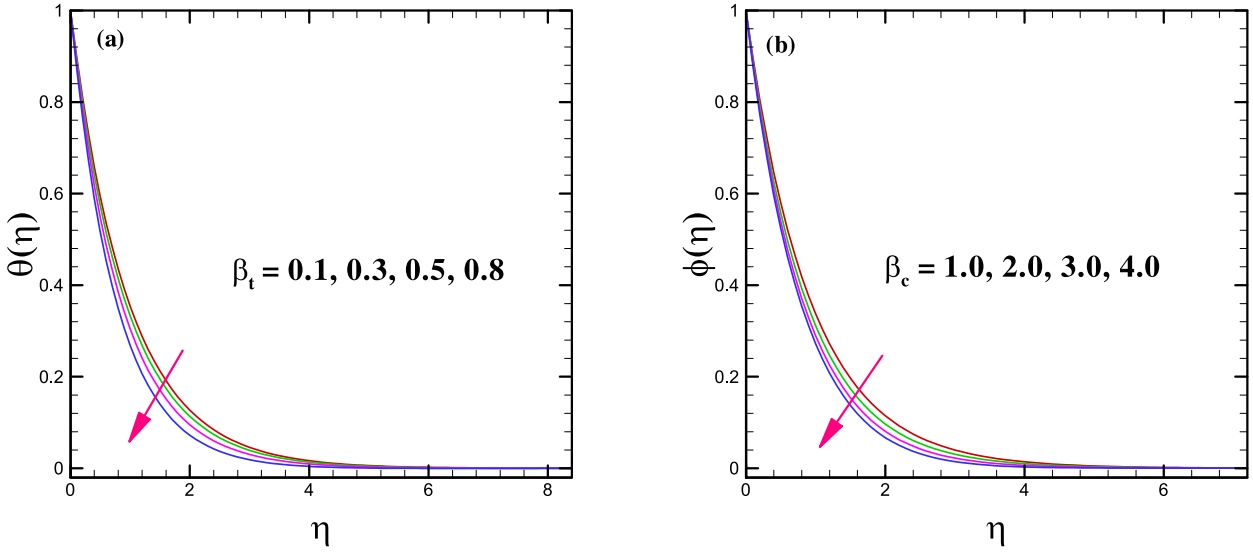

Fig. 6. (a-b): Impact of β_t and β_c on thermal and solutal profiles.

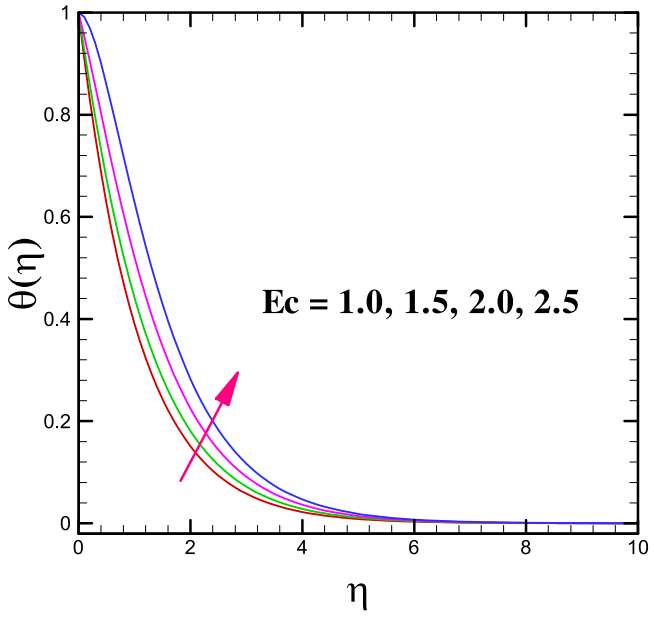

Fig. 7. Impact of Ec on temperature profile.

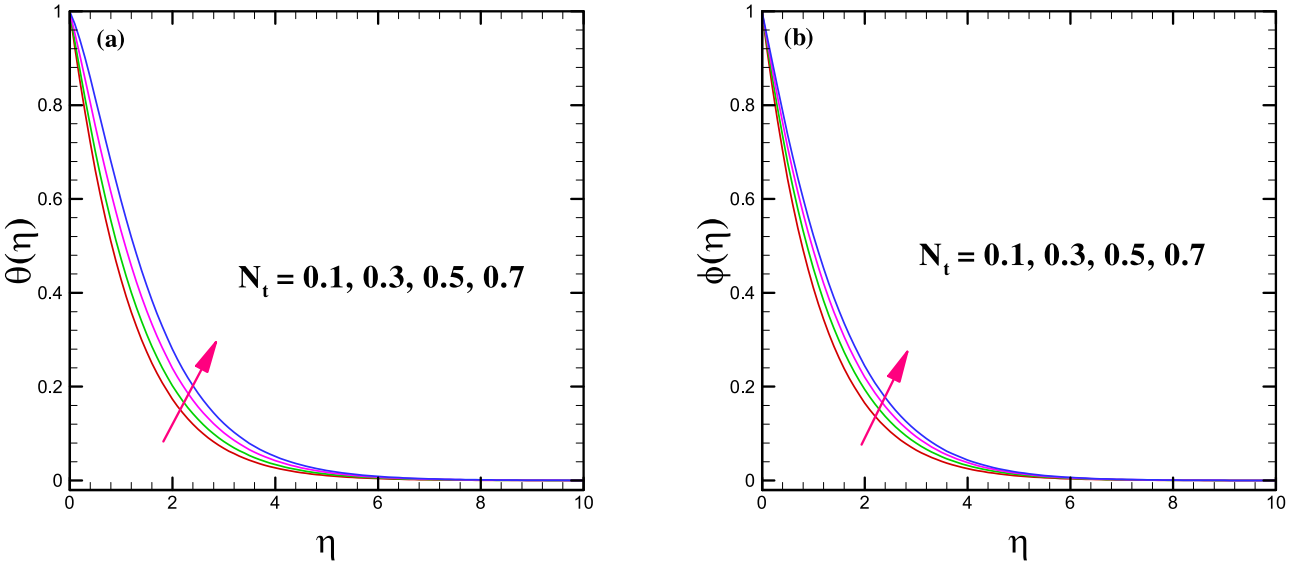

Fig. 8. (a-b): Impact of N_t on thermal and solutal profiles.

represented in plots. Moreover, the effect of Brownian motion constant (N_b) on thermal and concentration profiles of Burgers fluid is illustrated through Figures 9a and 9b. It is evident from these figures that transport of thermal energy in the flow shows the boosting trend while the nanoparticles concentration depreciates for amplifying values of (N_b). Due to Brownian motion, particles go under rapid motion due to which kinetic energy of the particles enhance which lead to magnify the thermal distribution of magnetized nanofluid. Since, the diffusion of nano-species is controlled by the Brownian motion hence, escalating amount of Brownian motion constraint depreciate the diffusion rate of nano particles and therefore the solutal curves of nanofluid diminish. Figure 10a exposes the consequence of Prandtl number (Pr) on transport of heat while, Figure 10b illustrates the stimulus of Schmidt number (Sc) for diffusion of mass in the system. The decay in the heat transfer rate is envisioned for magnifying values of Pr and the same trend is being detected for escalating amount of Sc on solutal energy transport curves. As, intensification in the strength of Pr enlarges the viscosity as well as the specific heat while the thermal conductivity of the liquid deteriorates in this regard as it can be observe from the relation, i.e, $Pr = \frac{\nu}{\alpha_1}$. Where, α_1 is the thermal conduction while, ν represents the momentum diffusivity. Also, note that here the heat transfers due

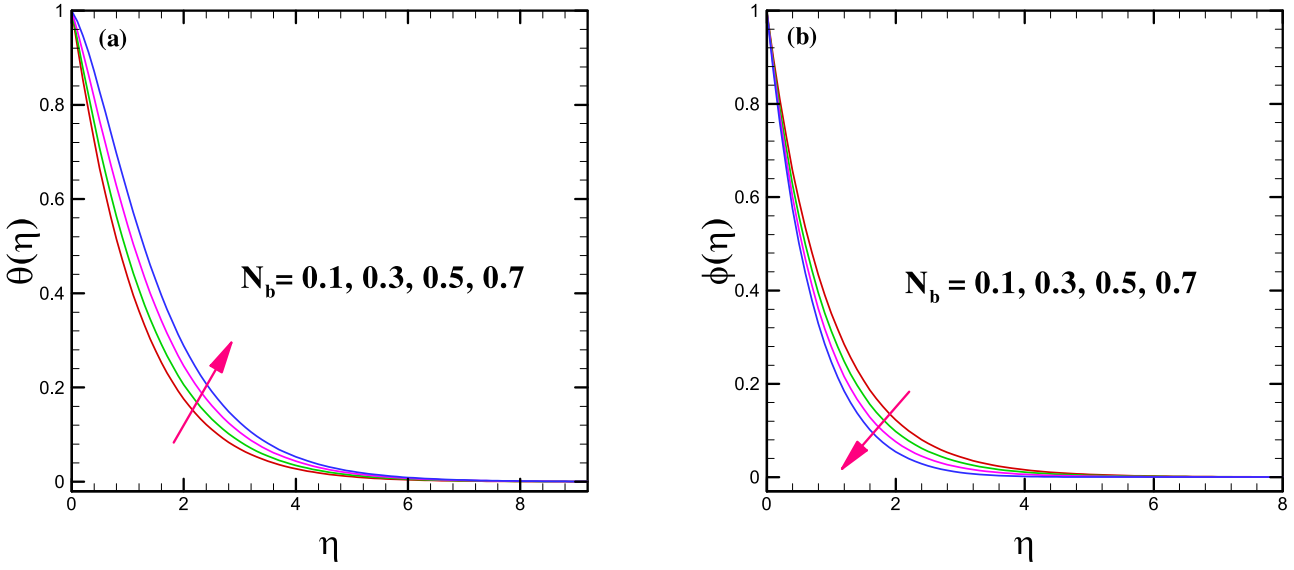

Fig. 9. (a-b): Impact of N_b on thermal and solutal profiles.

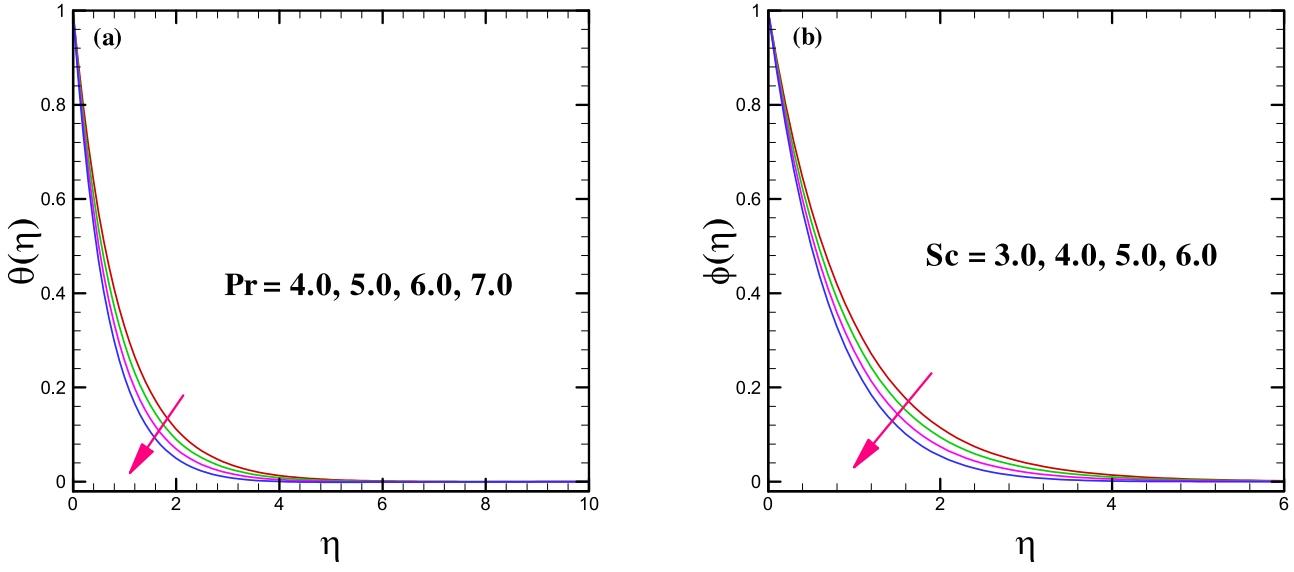

Fig. 10. (a-b): Impact of Pr and Sc on thermal and solutal profiles.

to convection. Moreover, a magnification in the intensity of Sc corresponds to decline the mass diffusion coefficient that's why nanoparticles concentration depreciates. We depicted Figures 11a, 11b to ensure the effect of hat source/sink variable for thermal curves of nanofluid. From these plots, it is clear that the thermal energy transport builds up in the flow for magnifying values of heat source constant ($\delta > 0$). On the other hand, it is seen that the thermal curves of nanofluid weakens for escalating amount of heat sink parameter ($\delta < 0$). Obviously, due to existence of heat source in the system the radiations produce extra amount of heat which magnify the temperature distribution and when heat sinks then temperature falls from the system. Hence, our theoretical outcomes are according to expectations. The influences of constructive and destructive chemical reaction parameters on solutal energy transport curves of nanofluid are demonstrated through Figures 12a, 12b. Depreciating trend of the mass diffusion curves is noticed for amplifying scales of constructive chemical reaction constant ($k > 0$) while diminishing trend is achieved for larger amount of destructive chemical reaction parameter ($k < 0$). Energy absorbs to some extent for execution of chemical reaction which leads to decline the solutal contours. Moreover, when the reaction rate deteriorates, the less magnitude of energy employs and system gain more energy to transfer therefore, transfer of solutal energy curves build up for larger values of destructive reaction parameter.

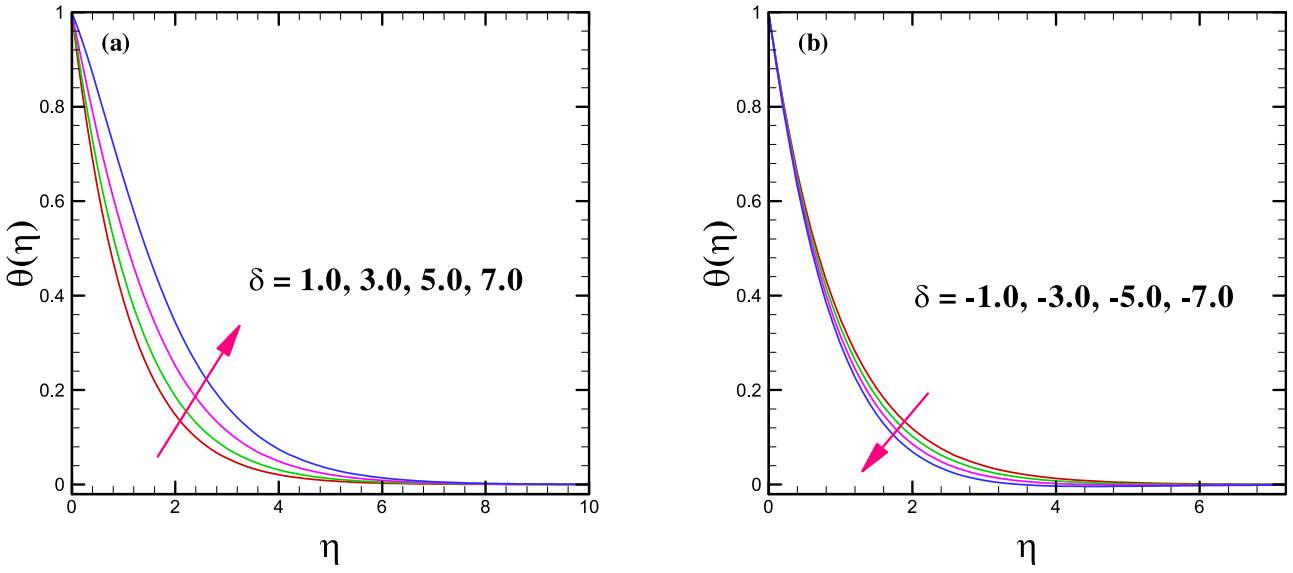

Fig. 11. (a-b): Impact of δ on temperature profile.

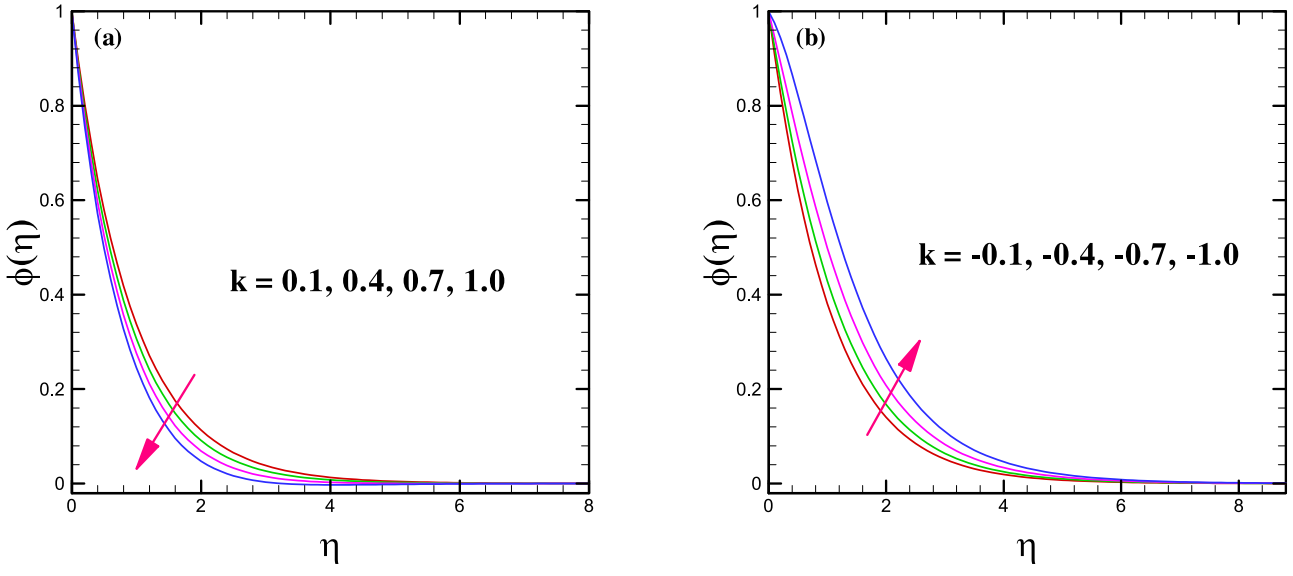

Fig. 12. (a-b): Impact of k on concentration profile.

6 Concluding remarks

The key points of the present study are listed below:

- the flow curves of Burgers nanofluid depreciate for magnifying values of fluid relaxation time constant while for fluid retardation time parameter these curves show intensification.
- Thermal and solutal energy transport curves depict contrast behavior to that of flow curves of Burgers nanofluid for magnifying scales of Burgers fluid parameter.
- The thermal contours of nanofluid strengthen for escalating values of Eckert number.
- Greater thermal and solutal relaxation times of nanofluid lead to diminish the thermal and solutal distributions of Burgers fluid, respectively.
- Nanoparticles concentration profile depicts ascending trend for boosting amount of thermophoretic force constant while for intensifying values of Brownian motion parameter it de-escalates.
- Growing values of heat generation constant builds up the heat transport in the flow while for increasing magnitude of heat absorption parameter heat transport found to falloff.
- Constructive chemical reaction leads to falloff the mass transport curves while destructive reaction enhances the mass transport in the flow of nanofluid.

Author contribution statement

Zahoor Iqbal: contributed in mathematical modelling simulation and writing the manuscript Masood Khan:

contributed in simulation and proof reading of the manuscript Awais Ahmed: helps in modelling and writing response to the referees comments.

References

1. P. Ravindran, J.M. Krishnan, K.R. Rajagopal, Int. J. Eng. Sci. **42**, 1973 (2004)
2. T. Hayat, C. Fetecau, S. Asghar, Int. J. Eng. Sci. **44**, 1423 (2006)
3. T. Hayat, Comput. Math. Appl. **52**, 1413 (2006)
4. M. Khan, S. Asghar, T. Hayat, Nonlinear Anal. Real World Appl. (2007)
5. T. Hayat, S. Ali, M. Awais, S. Obaidat, Prog. Computat. Fluid Dyn. Int. J. (2012), https://doi.org/10.1504/PCFD.2013.050650
6. T. Hayat, M. Waqas, M.I. Khan, A. Alsaedi, S.A. Shehzad, Chin. J. Phys. **55**, 318 (2017)
7. M. Khan, M. Irfan, W.A. Khan, Int. J. Mech. Sci. **130**, 375 (2017)
8. M. Waqas, M.I. Khan, T. Hayat, A. Alsaedi, Therm. Sci. **23**, 3425 (2019)
9. M. Khan, Z. Iqbal, A. Ahmed, Appl. Nanosci. (2020). https://doi.org/10.1007/s13204-020-01360-8
10. Z. Iqbal, M. Khan, A. Ahmed, J. Ahmed, A. Hafeez, Appl. Nanosci. (2020). https://doi.org/10.1007/s13204-020-01386-y
11. H. Masuda, A. Ebata, K. Teramae, N. Hishinuma, Netsu Bussei (Jpn) **4**, 227 (1993)
12. S.U.S. Choi, *Enhancing thermal conductivity of fluids with nanoparticles*, The proceedings of the 1995, in em ASME International Mechanical Engineering Congress and Exposition (ASME, San Francisco, USA, 1995), pp. 99–105
13. S.U.S. Choi, Z.G. Zhang, W. Yu, F.E. Lockwood, E.A. Grulke, Appl. Phys. Lett. **4**, 2252 (2001)
14. D.H. Yoo, K.S. Hong, H.S. Yang, Thermochim. Acta **9**, 455 (2006)
15. J. Buongiorno, J. Heat Transfer **128**, 240 (2006)
16. J. Philip, P.D. Shima, B. Raj, Appl. Phys. Lett. **92**, 043108 (2008)
17. W.A. Khan, I. Pop, Int. J. Heat Mass Transfer **53**, 2477 (2010)
18. M. Turkyilmazoglu, Chem. Eng. Sci. **84**, 182 (2012)
19. M. Turkyilmazoglu, J. Heat Transfer **136**, 031704 (2014)
20. M. Turkyilmazoglu, Comp. Fluids **94**, 139 (2014)
21. K.L. Hsiao, Comp. Fluids **104**, 1 (2014)
22. M. Sheikholeslami, R. Ellahi, Int. J. Heat Mass Transfer **89**, 799 (2015)
23. M. Sheikholeslami, Q.M.Z. Zia, R. Ellahi, Appl. Sci. **6**, 324 (2016)
24. K.L. Hsiao, J. Heat Mass Transfer **112**, 983 (2017)
25. K.L. Hsiao, Energy **130**, 486 (2017)
26. M. Sheikholeslami, R. Ellahi, K. Vafai, Alex. Eng. J. **57**, 565 (2018)
27. M. Sheikholeslami, M. Jafaryar, A. Shafee, Z. Li, J. Therm. Anal. Calorim. **134**, 2295 (2018)
28. M. Sheikholeslami, H. Sajjadi, A.A. Delouei, M. Atashafrooz, Z. Li, J. Therm. Anal. Calorim. **136**, 2477 (2019)
29. R. Ellahi, F. Hussain, S.A. Abbas, M.M. Sarfaraz, M. Goodarzi, M.S. Shadloo, *Study of two-phase Newtonian nanofluid flow hybrid with hafnium particles under the effects of slip, inventions* (2020). https://doi.org/10.3390/inventions5010006
30. A. Ahmed, M. Khan, J. Ahmed, A. Hafeez, Z. Iqbal, Arab. J. Sci. Eng. (2020). https://doi.org/10.1007/s13369-020-04468-9
31. T. Javed, M. Faisal, I. Ahmed, Case Stud. Therm. Eng. **21**, 100689 (2020)
32. A. Hafeez, M. Khan, J. Ahmed, Comp. Meth. Prog. Biomed. **191**, 105342 (2020)
33. M.S. Abel, J.V. Tawade, M.M. Nandeppanavar, Meccanica **47**, 385 (2012)
34. M. Irfan, M. Khan, W.A. Khan, J. Brazilian Soc. Mech. Sci. Eng. (2019). https://doi.org/10.1007/s40430-019-1619-9
35. M. Fathizadeh, M. Madani, Y. Khan, N. Faraz, A. Yildirim, S. Tutkun, J. King. Saud. Univ. Sci. **25**, 107 (2013)
36. A. Ahmed, M. Khan, M. Irfan, J. Ahmed, *Transient MHD flow of Maxwell nanofluid subject to non linear thermal radiation and convective heat transport* (2020). https://doi.org/10.1007/s13204-020-01375-1

Cite this article as: Zahoor Iqbal, Masood Khan, Awais Ahmed, Burgers fluid flow in perspective of Buongiorno's model with improved heat and mass flux theory for stretching cylinder, Eur. Phys. J. Appl. Phys. **92**, 31101 (2020)